RESEARCH/REVIEW ARTICLE

Effects of sea-ice light attenuation and CDOM absorption in the water below the Eurasian sector of central Arctic Ocean (>88°N)

Lars Chresten Lund-Hansen,[1,2] Stiig Markager,[3] Kasper Hancke,[4] Tanja Stratmann,[5] Søren Rysgaard,[2,6,7] Hans Ramløv[8] & Brian K. Sorrell[1,2]

[1] Aquatic Biology, Department of Bioscience, Aarhus University, Ole Worms Allé 1, Building 1134, DK-8000 Aarhus C, Denmark
[2] Arctic Research Center, Aarhus University, C.F. Møllers Allé 8, Building 1110, DK-8000 Aarhus C, Denmark
[3] Marine Ecology, Department of Bioscience, Aarhus University, Frederiksborgvej 399, DK-4000 Roskilde, Denmark
[4] Nordic Centre for Earth Evolution, Department of Biology, University of Southern Denmark, Campusvej 55, DK-5230 Odense M, Denmark
[5] Ecosystem Studies, Royal Netherlands Institute for Sea Research, Korringaweg 7, NL-4401 NT Yerseke, The Netherlands
[6] Greenland Climate Research Centre, c/o Greenland Institute of Natural Resources, DK-3900 Nuuk Greenland, Denmark
[7] Centre for Earth Observation Science, Department of Environment and Geography, University of Manitoba, Winnipeg MB R3T 2N2, Canada
[8] Department of Science, Systems and Models, Roskilde University, Universitetsvej 1, DK-4000 Roskilde, Denmark

Keywords
Sea ice; transmittance; PAR; CDOM; chl-a; Eurasian sector.

Correspondence
Lars Chresten Lund-Hansen, Aquatic Biology, Department of Bioscience, Aarhus University, Ole Worms Allé 1, Building 1134, DK-8000 Aarhus C, Denmark.
E-mail: lund-hansen@biology.au.dk

Abstract

This is a study of the optical, physical and biological parameters of sea ice and the water below it at stations ($n = 25$) in the central (>88°N) Eurasian sector of the Arctic Ocean during the summer 2012 record low sea-ice minimum extent. Results show that photosynthetically active radiation (PAR) transmittance of the ice was low (0.09) and apparently related to a high degree of backscattering by air-filled brine channels left by brine draining. The under-ice PAR was also low (8.4 ± 4.5 SD μmol photons m^{-2} s^{-1}) and partly related to the low transmittance. There were no significant differences in multi-year and first-year PAR transmittances. In spite of this low under-ice PAR, only 3% of the transmitted PAR through the ice was absorbed by phytoplankton in the water. On average, chlorophyll-a concentrations were low (0.34 ± 0.69 SD mg chl-a m^{-3}) in the water compared to the high ($a_{375} = 0.52$ m^{-1}) coloured dissolved organic matter (CDOM) absorption coefficient with a strong terrestrial optical signature. Two distinct clusters of stations with waters of Pacific and North Atlantic origin were identified based on significant differences in temperature, salinity and CDOM absorption coefficient between water masses. The under-ice light field for bare ice was parameterized as follows: $I_z = I_o(1 - 0.55)*(0.09)*\exp^{(-0.17*z)}$.

The Arctic sea-ice extent has been decreasing gradually since at least 1978 (Parkinson et al. 1999), when the appropriate remote sensing tools first became available. A minimum of 4.0×106 km^2 was recorded in 2007 (Maslanik et al. 2007; Kwok & Rothrock 2009), followed by an even lower minimum of 3.1×106 km^2 in August 2012 (Parkinson & Comiso 2013). This decline has been attributed to general global warming (Maslanik et al. 2007), increased inflow of warm Atlantic water to the Arctic Ocean supplying energy to the area (Rudels et al. 2004) and wind-driven increased transport of sea ice out of the Arctic Ocean through the Fram Strait (Rigor & Wallace 2004; Ogi & Rigor 2013). Studies have further shown that the thickness of the sea ice in the Arctic Ocean has decreased significantly and that the percentage of first-year ice (FYI) has increased at the expense of multi-year ice (MYI; Rothrock et al. 1999; Rigor & Wallace 2004; Stroeve et al. 2005). It is foreseen that a significantly thinner sea ice and a change to predominant FYI will increase the transmittance of heat and light to the water column below the ice (Nicolaus et al. 2012). Primary production is very low (4–5 mg C m^{-2} day^{-1}) in the

Citation: *Polar Research* 2015, *34*, 23978, http://dx.doi.org/10.3402/polar.v34.23978

central Arctic Ocean (Sakshaug 2004; Popova et al. 2012; Boetius et al. 2013), and it is assumed to be limited mainly by light, at least during spring and early summer (Sakshaug 2004). A higher transmittance and irradiance below the ice, and in newly ice-depleted areas, may therefore increase primary productivity of both ice algae attached to the bottom of the sea ice and phytoplankton living in the upper part of the water column (Arrigo et al. 2008; Zhang et al. 2010; Arrigo et al. 2011). However, ice algae, which contribute about 10–20% of the primary production in the central Arctic Ocean (Arrigo et al. 2008), are acclimated to very low light levels of 5–15 μmol photons m^{-2} s^{-1} at the bottom of the ice (Thomas & Dieckmann 2002; Arrigo et al. 2008). Ice algae remain spatially fixed at varying but high daily summer light levels, whereas pelagic phytoplankton mix vertically up and down through a strong light gradient in the water column below the ice. The consequences of thinning sea ice for the light climate experienced by Arctic algae need greater understanding given the rapid change in ice thickness and cover. The following questions will be addressed: (1) Are there any changes in ice thickness between the present and previous data set?; (2) To what degree is photosynthetically active radiation (PAR) transmittance governed by ice thickness?; (3) What governs PAR attenuation in the water below the ice?; (4) How much of the light is utilized by the phytoplankton?; and (5) Is there any specific spatial variation in optical and water parameters as temperature and salinity? The spatial sampling resolution of the present study is high in parts of the Arctic Ocean ($>88^{\circ}$N) that were previously investigated based on cross-polar transects with limited spatial resolution (Gosselin et al. 1997; Tucker et al. 1999).

Methods and data

Sea-ice cores

Transport to all stations was accomplished by helicopter from the icebreaker *Oden*. A typical sampling station was selected from a height of about 100 m above the ice as far from pressure ridges, leads, hummocks and open waters as possible. After landing on the ice, the deteriorated ice that covered the surface was removed until the solid ice surface was reached, and the thickness of the deteriorated layer was measured to the nearest 1 cm. At each station, two to four cores were sampled with a Mark II (90 mm) coring system (Kovacs Enterprise, Roseburg, OR, USA), and the length of cores measured to the nearest 1 cm. The horizontal distance between the cores was about 2–3 m. One core, selected for temperature profiling, was immediately placed in a horizontal cradle and the temperature was measured in drilled holes (5 mm) of the core every 5 cm with a digital thermometer to nearest 0.1°C. The bottom 5 cm of this core was cut off, sealed in a polyethylene bag and placed in a cooling box for transportation to the ship, where it was thawed. A second core was cut into 10 cm slices and each slice sealed in a polyethylene bag and stored in a cooling box for transportation. Loss of material due to core chipping and brine drainage was kept to a minimum by careful handling of the samples but could not always be avoided. The exact length of each of the 10 cm slices was measured with a calliper to the nearest 0.1 cm and weighed with a digital scale to the nearest 1 g immediately after transport to the ship. Each slice was left for melting overnight (24 h) in bottles with lids before conductivity and temperature of the meltwater was measured with a YK-2004CD meter (Lutron, Taipei, Taiwan) and converted into salinity using the Fofonoff & Millard (1983) relations. Air and brine volumes were derived through the Cox & Weeks (1983) relations with F1(T) and F2(T) for temperatures higher than -2°C (Leppäranta & Manninen 1988). Water from below the ice for chlorophyll-a (chl-a) and coloured dissolved organic matter (CDOM) absorption coefficient was sampled in cleaned polyethylene canisters using a bilge pump mounted with a hose, which was lowered through a hole in the ice to a depth of about 50 cm below the ice. An exact volume of water both from the 5 cm slice from the bottom of the ice core and from the water below the ice was filtered through GF75 glass fibre filters (Advantec, Tokyo, Japan) with a nominal size of 0.3 μm, using a vacuum of maximally 30 kPa (0.3 bar). Separate filters were used for measurements of chl-a concentration and particulate absorption. Filters for chl-a were packed individually in aluminium foil bags and stored in a freezer at -18°C. In the laboratory in Denmark, filters were kept in 5 ml 96% ethanol at 5°C for a minimum of six and a maximum of 20 h for pigment extraction from the retained algae. Samples were centrifuged and the fluorescence of the supernatant was measured with a TD-700 fluorometer (Turner Design, Sunnyvale, CA, USA) and converted into chl-a concentrations by a calibration of the fluorometer. Under-ice video recordings were obtained by mounting a Lumix DMC FT5 underwater camera (Panasonic, Osaka, Japan) on an iron pole. The camera was lowered through an ice core hole to the bottom of the ice for inspection of under-ice conditions. Temperature data were obtained by lowering a conductivity–temperature–depth (CTD) Plus 100 Sensor (SiS, Schwentinental, Germany) through the hole from where the ice core was retrieved with a vertical resolution of 0.1 m to a depth

Citation: *Polar Research* 2015, *34*, 23978, http://dx.doi.org/10.3402/polar.v34.23978

of 25 m. Salinity of sampled water (50 cm below ice) was determined by measuring conductivity because the conductivity censor on the CTD Plus 100 malfunctioned. The ice cores were classified as MYI or FYI, where a higher bulk salinity (3–4) and a more pronounced change in this salinity distinguish FYI from MYI, where low salinities (1–2) are also a typical characteristic (Warner et al. 2013).

Spectral chl-a absorption and CDOM

Spectral light absorption by particles (350–750 nm with 1 nm interval) was measured with the filter pad method (Kishino et al. 1985) using a UV-2401PC UV-Vis recording spectrophotometer (Shimadzu Corporation, Kyoto, Japan) equipped with an integrating sphere-type ISR-240A as described by Stæhr & Markager (2004). Samples of 300 ml were filtered on GF-F filters (0.7 μm) and stored at −80°C before measuring in the laboratory in Denmark. However, for some samples less than 300 ml were available and the optical density was close to the detection limits for parts of the spectrum. The absorption spectral coefficients were calculated according to Cleveland & Weidemann (1993). We found that their equation for a β-factor was the most reliable at low optical densities. The spectral absorption coefficients were then divided into absorption due to pigments and detritus according to Bricaud & Stramski (1990). The CDOM samples were filtered through GF-F filters (0.7 μm) and were kept in the dark at 5°C until they were analysed after arrival back at the laboratory in Denmark. Samples were allowed to warm to room temperature before analysis and absorption was measured on a Shimadzu UV-24101PC UV-Vis recording spectrophotometer with a 10 cm quartz cuvette from 700 to 240 nm with 5 nm intervals. Milli-Q water was used as a reference and the CDOM absorption coefficient at 375 nm (a_{375}) and slope (S) were calculated according to Stedmon & Markager (2001).

Optics

An Li-190 PAR (400–700 nm) sensor (LI-COR, Lincoln, NE, USA) was mounted at the bow of the ship to record surface downwelling PAR during the cruise. The sensor was connected to a CR-10 data logger (Campbell Scientific, Logan, UT, USA) with recording every 5 min. Sea-ice PAR transmittance t was determined as $t = (I_i/(1-\alpha)*I_d)$, where I_d and I_i are irradiances at the surface and below the ice and α the albedo. The PAR attenuation coefficient of the ice K_d(PAR)ice was determined as $K_d(\mathrm{PAR})\mathrm{ice} = \ln((I_i/(1-\alpha)*I_d))/z$, where z is the ice thickness (m). The albedo here is taken as $\alpha = 0.55$ based on a whole season of in situ measurements of albedo at 88°N during a summer and late summer season (Vihma et al. 2008), where the areal extent and consistency of the albedo has been demonstrated by satellite *reconnaissance* (Riihelä et al. 2010). PAR irradiances were measured with a recently calibrated LI-COR Li-192 sensor. The sensor was mounted on a thin dark-painted metal stick and lowered through a 9 cm diameter hole to the bottom of the ice. The hole was filled with small pieces of ice from the drilling to avoid any false surface light entering the hole. Care was taken to avoid any shadow effects from the stick in case of direct sun, and leaving the surface as undisturbed as possible, with no footprints. The first readings were immediately below the ice to determine the sea-ice PAR transmittance. This was followed by subsequent readings at 0.1 m intervals covering a distance of 1.5–2.0 m in the water below the ice. An average of 10 readings was obtained at each depth below the ice and data were used for determining the PAR attenuation coefficient K_d(PAR) in the water below the ice. Downwelling PAR in the air at the surface was measured both before and after under-ice measurements to check for changes in irradiance during measurements, which lasted 5–10 min each. The attenuation coefficient K_d(PAR) was derived through linear regression of the log-transformed PAR readings. The linear regression model described the PAR data very well (r^2 ca. 0.97) in accordance with $I_z = I_I\, e^{-K_d(\mathrm{PAR})*z}$, where I_z is the irradiance (μmol photons m^{-2} s^{-1}) at depth (m) z, I_I is here the irradiance just below the ice and K_d(PAR) is the attenuation coefficient (Kirk 1994). The spectral distribution of downwelling ($E_d(\lambda)$) irradiance in the air and below the ice was obtained by means of a TriOS irradiance sensor (Rastede, Germany), which measures the spectra between 320 and 950 nm with a 3.3 nm resolution. A hole with a diameter of 25 cm was drilled through the ice and spectral sensor was lowered to a depth below the ice. Here a mechanical L-arm raised the sensor into a horizontal position and the sensor was lifted to measure immediately below the ice. The length of the arm was 75 cm and the hole was carefully filled with small chunks of ice and snow in order to avoid any false surface light interfering with measurements. Ten to 12 readings were obtained at measurement depths 0–2 m below the ice with sensor integration time from several milliseconds to a few seconds. Surface spectral irradiance in air was measured immediately before and after completing under-ice measurements. All data were obtained within about 10 min. $K_d(\lambda)$ was derived as $K_d(\lambda) = \ln(E_z(\lambda)/E_z - 1(\lambda))/(z - z - 1)$, with $E_z(\lambda)$ as irradiance at a specific wavelength (λ) and depth (z).

Results and discussion

Sea-ice conditions: summer 2012

The lowest Arctic sea-ice extent ever recorded since 1978 of ca. 3.1×106 km^2 was reached in mid-September 2012, notably lower than the previous 2007 minimum of ca. 4.2×106 km^2 (Parkinson & Comiso 2013). The Kara, Laptev and Chukchi seas as well the western Beaufort Sea were nearly ice-free, whereas the eastern Beaufort Sea, the oceans north and east of Greenland, and the North Pole area remained ice-covered. The LOMROG III cruise to the Arctic Ocean started on 31 July from Longyearbyen, Svalbard, and ended there on 14 September 2012. We sampled at 25 ice core stations 226–255 (Julian days), of which 21 stations were located in the central Arctic Ocean ($>88^\circ$N, Fig. 1). Melt ponds of variable sizes were present at all stations but most of those in the central Arctic Ocean were refrozen and covered with a 1–2 cm thick layer of new ice during sampling in the central Arctic from 10 August onwards. The layer of new ice on the melt ponds reached a thickness of about 10 cm around 5 September, when central Arctic sampling was completed. No direct quantitative measurements of melt pond coverage were made, but coverage varied between stations. A photograph taken at station 227 on 14 August shows a typical ice surface with frozen melt ponds in the background and the layer of deteriorated ice from station 246 (Fig. 2). The width of the ice core is 90 mm. An under-ice video recorded at station 247 can

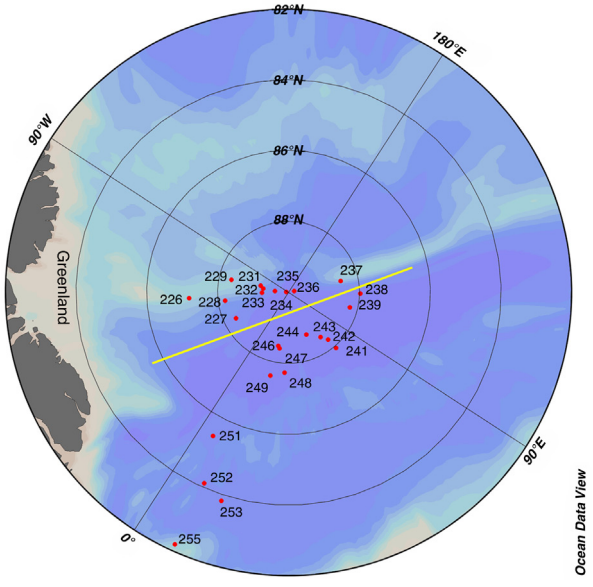

Fig. 1 Central Arctic Ocean with stations named from Julian days. The yellow line demarcates the water masses of Pacific origin above the line and of Atlantic origin below.

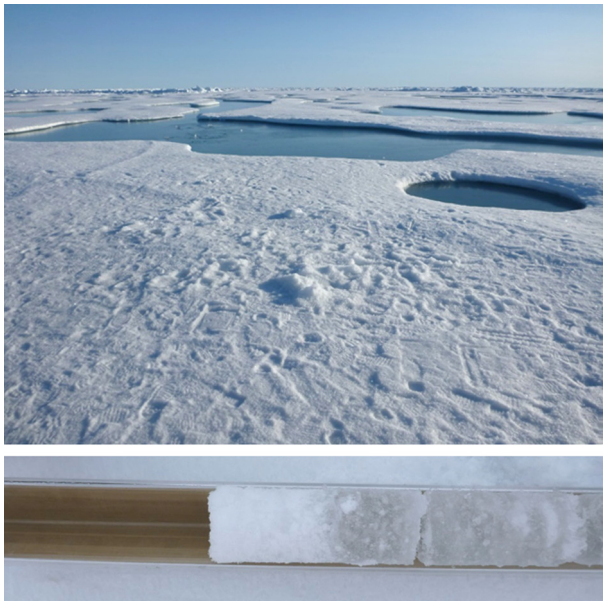

Fig. 2 Station 227 on 14 August with frozen melt ponds and the top of the ice core with a clear layer of deteriorated ice from station 246.

be seen at www.youtube.com/watch?v=B7VhofajmqE. Under-ice video recordings were obtained at stations 246–255 (Fig. 1), which all showed clear signs of bottom ablation as small crevasses, minor burrows and holes. A total of 15 ice cores (65%) were classified as MYI and 8 (23%) as FYI and 2 could not be classified but with no clear spatial pattern among stations (Fig. 1). Sea-ice temperature, bulk salinity, density, brine, and air volume are shown for two representative ice cores from stations 226 (MYI) and 237 (FYI, Fig. 3), where especially the higher bulk salinity, and a distinct change in this salinity, distinguish FYI from MYI (Warner et al. 2013). The lower bulk salinity in MYI is the result of salt ejection and brine drainage processes going on for a longer time compared to FYI. Average bottom sea-ice temperatures for all cores ($n = 25$) were ca. -2.0 ± 0.5 (SD) $^\circ$C, and average sea-ice top surface temperatures of -1.0 ± 0.5 (SD) $^\circ$C. Air temperatures recorded on *Oden* were close to freezing point between 19 and 30 August and thereafter were ca. -1.7°C until the end of the cruise on 10 September. The sky was completely overcast but with a good to fair visibility at all stations, except for stations 226, 227 and 228, where there were clear skies. All physical, optical and biological data from all stations are shown in Table 1.

Sea-ice thickness, bulk salinity, temperature and density

Average sea-ice thickness was 160 ± 33 (SD) cm except for a few long (272 cm) and short (107 cm) cores, with no clear spatial pattern (Fig. 4a). Note that ice thickness

Citation: *Polar Research* 2015, *34*, 23978, http://dx.doi.org/10.3402/polar.v34.23978

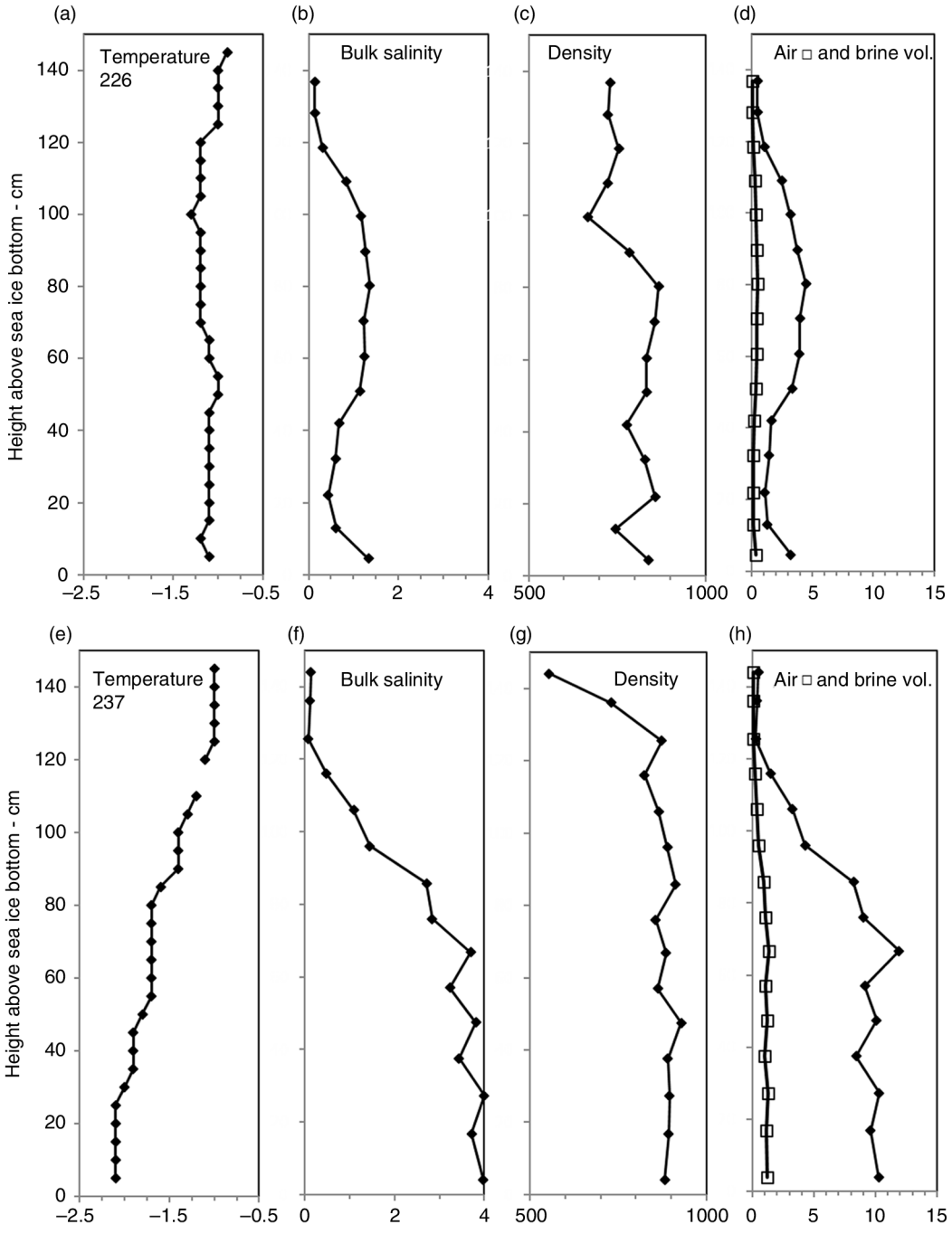

Fig. 3 Temperature (°C), bulk salinity, density (kg m^{-3}), brine and air volume (%) at station 226 representing (a–d) multi-year ice and (e–h) station 237 representing first-year ice.

here also includes the surface layer of deteriorated ice (see below). The variation in ice thickness between ice cores within each station was low (±4 cm), as determined by length measurements of two cores at most stations ($n = 21$) and 3–4 cores at four stations. The snow-free ice surface consisted of deteriorated ice with an average ($n = 23$) thickness of 9.0±3.0 (SD) cm at stations 226–249, whereas a layer of 10–12 cm thick snow covered the ice surface at stations 253 and 255. Satellite-based sea-ice thickness data from the North Pole region from 2003 to 2007 gave an average of 1.90 m (Kwok & Rothrock 2009). The present average of 1.60 m therefore indicates a

Table 1 Station identification number (Julian day), position, K_d(photosynthetically active radiation [PAR])$_i$ (m^{-1}) of the ice, $K_d(PAR)_w$ (m^{-1}) of the water, transmittance (%), PAR (µmol photons m^{-2} s^{-1}) under-ice, chl-a (mg chl-a m^{-3}) in the water, chl-a (mg chl-a m^{-2}) in the ice, coloured dissolved organic matter (CDOM) absorption coefficient a_{375} (m^{-1}) in the water, freeboard of the ice (cm), thickness of deteriorated ice (cm) and ice thickness (cm). M signifies multi-year ice and F signifies first-year ice.

ID	Latitude	Longitude	K_d— ice (m^{-1})	K_d— water (m^{-1})	Trans. (%)	PAR under ice (µM m^{-2} s^{-1})	Chl-a water (µg chl-a l^{-1})	Chl-a ice (mg chl-a m^{-2})	a_{375} (m^{-1})	Free-board (cm)	Deteriorated ice (cm)	Ice thickness (cm)
226	87 11.70°N	53 35.52°W	1.44	0.25	10.2	17.6	0.19	0.01	0.649	10	7	158 M
227	88 20.80°N	30 45.96°W	1.51	0.15	7.5	16.9	0.06	0.04	0.452	14	8	171 F
228	88 11.83°N	49 35.09°W	1.37	0.31	10.2	18.1	0.08	0.02	0.603	15	6	166 F
229	88 20.85°N	69 36.42°W	1.27	0.22	12.2	11.2	0.13	0.01	0.639	–	6	167 F
231	89 15.36°N	56 16.46°W	1.30	0.19	13.8	11.3	0.12	0.01	0.687	8	8	153 M
232	89 11.39°N	70 50.09°W	1.72	0.17	8.2	10.2	0.11	0.02	1.027	11	10	145 M
233	89 16.79°N	65 27.15°W	1.36	0.18	2.4	1.64	0.16	0.01	0.913	15	8	272 F
234	89 56.11°N	73 41.69°W	1.36	0.25	12.2	8.5	0.12	0.02	0.711	15	7	154 M
235	89 37.19°N	62 16.44°W	1.43	0.18	11.5	12.3	0.18	0.02	0.859	9	8	151 M
236	89 50.23°N	135 55.34°E	1.69	0.19	12.4	14.0	0.13	0.01	0.565	8	8	123 M
237	88 30.06°N	135 34.56°E	1.57	0.18	7.8	8.4	0.17	0.01	0.828	16	10	163 F
238	87 58.55°N	122 09.07°E	1.19	0.09	12.7	8.5	0.10	0.01	0.594	9	10	174 F
239	88 13.15°N	109 25.26°E	1.59	0.09	9.3	5.7	0.15	0.01	0.540	10	14	149 M
241	87 56.55°N	73 29.39°E	1.09	0.19	13.8	5.2	0.05	0.01	0.340	10	15	182 M
242	88 15.64°N	72 51.76°E	1.36	0.07	10.4	9.6	0.10	–	0.343	12	20	166 M
243	89 27.29°N	68 26.98°E	1.76	0.13	10.9	7.6	0.22	0.01	0.352	5	11	126 M
244	88 42.75°N	55 56.35°E	1.58	0.07	8.4	6.1	0.25	0.05	0.387	–	8	156 M
246	88 28.19°N	22 18.17°E	1.68	0.22	6.7	8.0	0.50	0.37	0.413	15	10	161 M
247	88 24.37°N	23 50.83°E	1.53	0.08	8.9	8.0	0.30	0.60	0.477	19	7	158 –
248	87 44.35°N	30 05.51°E	2.01	0.09	5.1	3.0	0.32	0.29	0.406	10	8	148 –
249	87 35.96°N	20 37.56°E	1.75	0.31	1.8	1.2	0.21	0.52	0.415	15	10	230 M
251	85 25.63°N	05 15.95°E	1.57	0.17	8.4	6.5	0.24	0.11	0.303	10	7	157 M
252	84 07.26°N	09 11.02°E	1.64	0.14	10.4	2.7	0.10	0.04	0.238	11	8	130 F
253	83 49.45°N	15 08.02°E	–	0.09	–	4.6	3.50	0.06	0.040	11	–	107 F
255	82 11.69°N	08 41.81°E	–	0.29	–	2.3	1.02	0.08	0.178	14	–	145 M

thinning of the sea ice in the central Arctic Ocean, keeping in mind that the 2003–07 data are based on remote sensing. Visual inspection of the ice cores showed no observable sediments and there were also no visible sediments left on the chl-a filters after filtration that might affect transmittance. However, areas and patches of dirty sea ice were sometimes observed from the *Oden* but were not quantified.

PAR transmittance, K_d(PAR)ice and albedo

Average PAR transmittance (t) reached 0.09 ± 0.03 (SD) but with no significant spatial variation between stations (Fig. 4b) and no significant differences in average transmittance between MYI (0.10 ± 0.03 SD) and FYI (0.08 ± 0.03 SD). Nevertheless, the slightly higher MYI transmittance is in accordance with results of a comprehensive study of FYI and MYI optical properties (Light et al. 2008). Note that present results only apply for sea-ice transmittance where the significant increase in transmittance from 0.02 in MYI to 0.11 in FYI demonstrated by Nicolaus et al. (2012) was quantitatively more related to higher melt pond coverage in FYI. The correlation between sea-ice thickness and ln (PAR transmittance) was here fairly high ($r^2 = 0.55$, $n = 23$) but relied entirely on two data points of thick ice (Fig. 5) where $r^2 = 0.01$ without these two points. The range in ice thickness was limited (160 ± 33 SD cm) which indicates that the absence of a clear and strong correlation might be related to the low variation in ice thickness. It is the absorption and especially the scattering by brine channels and air bubbles that reduce transmittance in sea ice (Perovich 1996; Hamre et al. 2004). A comparison of air and brine volumes in the MYI (station 226) and FYI (station 237) cores (Fig. 3d, h) shows a notably higher (ca. 10%) brine volume in the lower part of the FYI core compared to the MYI cores (5%), but transmittance was insignificantly higher in MYI ($\tau = 0.10$) compared to FYI ($\tau = 0.08$). It might accordingly be expected that transmittance was higher for the MYI with the lower brine volume but scattering depends also on the phase function, which, although unknown here, describes the angular direction of the scattered light (Hamre et al. 2004). Salt drainage from the brine channels can occur in warm sea ice with temperatures just below the freezing point (Perovich et al. 1993). Brine channels then fill with

Citation: *Polar Research* 2015, *34*, 23978, http://dx.doi.org/10.3402/polar.v34.23978

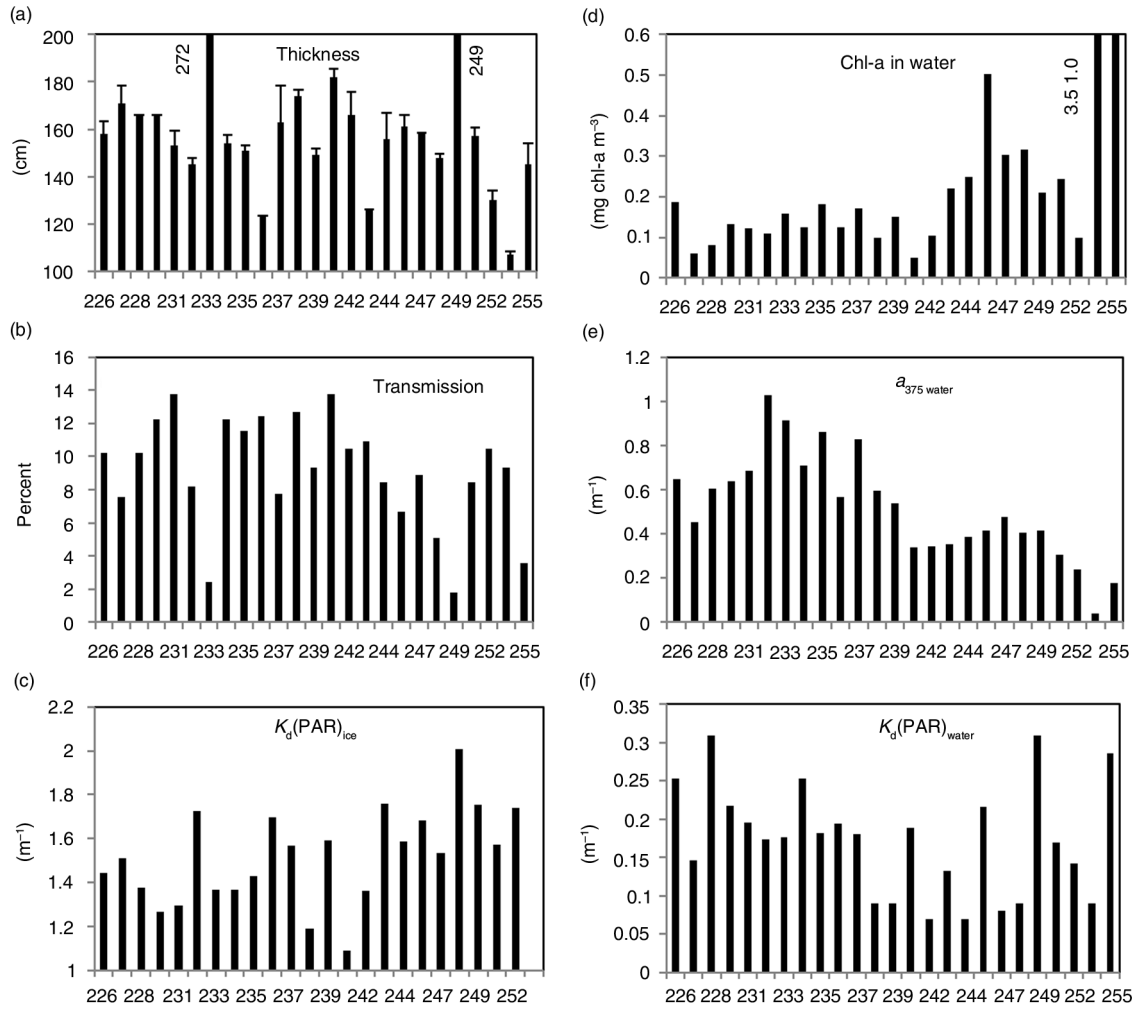

Fig. 4 (a) Ice thickness (cm), (b) photosynthetically active radiation (PAR) transmittance (τ,%), (c) diffuse attenuation coefficient K_d(PAR) (m^{-1}) of the ice, (d) chl-a (mg chl-a m^{-3}) in water below ice, (e) coloured dissolved organic matter (CDOM) absorption coefficient—a_{375} (m^{-1}) in water, and (f) diffuse attenuation coefficient K_d(PAR) (m^{-1}) in the water.

air, which increases the backscattering coefficient and thereby decreases transmittance (Hamre et al. 2004). However, the average PAR transmittance of 0.09 measured for bare ice in the present study is similar to those observed in the Barents Sea (Sakshaug 2004), but it is slightly lower compared with a transmittance of 0.13 in land-fast ice in Kangerlussuaq fjord, West Greenland (Hawes et al. 2012). These ice cores were cold (-8 to -10°C) with low brine volumes and no salt drainage. The PAR attenuation coefficient of the present ice cores—K_d(PAR)ice—reached an average of 1.51 ± 0.22 (SD) m^{-1} with a high (1.09–2.01 m^{-1}) range. These values are quite higher compared to the ranges of 1.1–1.5 m^{-1} of Perovich (1996), and the 0.9 m^{-1} of a 1.5 m thick north-east Greenland ice (Glud et al. 2007). It is accordingly supposed that the low transmittance and the high PAR attenuation in the ice were related to air-filled brine channels and increased scattering due to low ice temperatures. However, applying a constant albedo ($\alpha = 0.55$) in deriving the sea-ice PAR transmittance and attenuation coefficients—K_d(PAR)ice—might

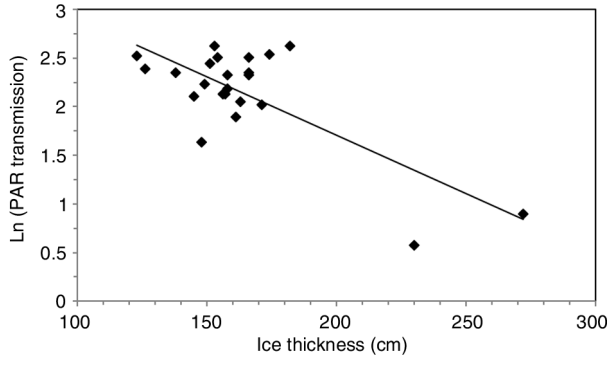

Fig. 5 Ice thickness (cm) versus ln (photosynthetically active radiation [PAR] transmittance).

cause some uncertainties but the following sensitivity analysis shows that these are small. For instance, transmittance was 6.7% for $\alpha = 0.55$ at station 246, which increased to 8.5% for $\alpha = 0.65$ and decreased to 5.5% for $\alpha = 0.45$. Similar for the PAR ice attenuation $K_d(PAR)ice = 1.79\ m^{-1}$ at station 246, which increased to $1.93\ m^{-1}$ for $\alpha = 0.45$ and $1.63\ m^{-1}$ for $\alpha = 0.65$. This chosen albedo range (0.45–0.65) is comparatively high for a bare and level sea-ice surface (Light et al. 2008), where the effects of a constant albedo are there but limited. However, the flaky and unconsolidated deteriorated ice covering the surface of the ice probably also affected the transmittance, though there are to our knowledge no studies of the optical properties of this layer regarding its transmittance. Under-ice PAR decreased gradually from 17.7 µmol photons $m^{-2}\ s^{-1}$ at station 226 (13 August) to 2.3 µmol photons $m^{-2}\ s^{-1}$ at station 255 (11 September). The under-ice PAR level depends, in addition to the transmittance, also on atmospheric conditions, albedo and time of day and year, whereby the observed decrease in under-ice PAR is related to a decreasing solar angle over time between mid-August and mid-September. Nevertheless, average under-ice PAR of 8.4 ± 4.5 (SD) µmol photons $m^{-2}\ s^{-1}$ compares to measurements in the central Arctic Ocean also carried out in August–September 2012 (Boetius et al. 2013).

In the water below the ice—$K_d(PAR)_w$ chl-a and CDOM

An average attenuation coefficient $K_d(PAR)_w$ in the water below the ice of 0.17 ± 0.07 (SD) m^{-1}, with a range between 0.07 and $0.31\ m^{-1}$, was observed. This is similar to values obtained in other Arctic marine waters, often when there is a strong dependence on chl-a concentrations (Sakshaug 2004). Average chl-a in the water below the ice was low (0.35 ± 0.69 mg chl-a m^{-3}), with a range of 0.05–3.5 mg chl-a m^{-3}, and these values are also comparable to other Arctic waters (Gosselin et al. 1997; Ardyna et al. 2013). The particular high value of 3.5 mg chl-a m^{-3} was supposedly caused by a clump of *Melosira*. The average CDOM absorption coefficient $a_{375} = 0.52 \pm 0.24$ (SD) m^{-1}, with a range from 0.04 to $1.04\ m^{-1}$, compares also to previous observations in the Arctic Ocean (Granskog et al. 2012). It is interesting to note that both $K_d(PAR)w$ and a_{375} are quite similar to those observed in temperate and tropical freshwater-influenced estuaries (Lund-Hansen 2004; Lund-Hansen et al. 2013). However, spatial analyses showed that the CDOM absorption coefficient a_{375} was significantly ($p < 0.001$) higher (0.72 ± 0.17 SD m^{-1}) at stations 226–237 compared to the 238–255 group (0.32 ± 0.12 SD m^{-1}), with a clear demarcation separating the two groups (Fig. 1). Salinities were also significantly ($p < 0.001$) lower (< 27.0 PSU) at stations 226–237 and temperatures significantly higher (-1.638 ± 0.037 SD °C) compared to stations 238–255, where salinities were higher (> 27.0 PSU) and water temperatures lower (-1.773 ± 0.014 SD °C). A tendency of a lower chl-a at stations 226–237 (0.13 ± 0.04 SD mg chl-a m^{-3}) as compared to 238–255 (0.57 ± 0.95 SD mg chl-a m^{-3}) was neither statistically significant ($p < 0.001$) nor were any of the other parameters. The line between station groups shown in Fig. 1 corresponds with the Polar Front boundary between water masses of Pacific and Atlantic origin (Schauer et al. 2002; Aagaard et al. 2006) as also shown from nutrient and CTD data (Jones et al. 2008), which locates stations 226–237 in the Pacific and stations 238–255 in the Atlantic realm. The present samples were collected in the Polar Mixed Layer, a layer about 30 m thick lying below the ice in the Arctic Ocean which is affected by freshwater (river) inflow, melting and freezing of the ice (Rudels et al. 2004). To our knowledge, this is the first time that the Polar Front has been identified by sampling just below the ice in the Arctic Ocean and it demonstrates that there must be a considerable mixing between Polar Mixed Layer and lower lying water masses. Analyses of CDOM data using the Stedmon & Markager (2001) model showed that CDOM at all stations had a significant and strong terrestrial origin, which points towards the Russian rivers as the main source, as opposed to an autochthonous or oceanic origin. There were no significant differences between stations in $K_d(PAR)_w$ as outlined, and an average $K_d(PAR)_w$ was applied in the parameterization of the under-ice light field applicable in models of primary production in the Arctic Ocean (Arrigo et al. 2008; Zhang et al. 2010). PAR with water depth is: $I_z = I_o \exp^{(-K_d(PAR)*z)}$ with I_z and I_o as PAR at depth and surface, and $K_d(PAR)_w$ the attenuation coefficient with z as depth (Kirk 1994). For a water column below sea ice with a specified albedo (α) and transmittance (τ), the equation is: $I_z = I_o(1 - \alpha)*(\tau)*\exp^{(-K_d(PAR)w*z)}$, where I_o is the PAR irradiance at the surface of the ice. For the central Arctic Ocean, with an average transmittance of 0.09, an average $K_d(PAR)_w$ of $0.17\ m^{-1}$ and the albedo of 0.55, this equals: $I_z = I_o(1-0.55)*(0.09)*\exp^{(-0.17*z)}$. The relation only applies for snow-free and bare ice conditions, where primary production is high both below the ice and in the waters of the Arctic Ocean (Arrigo et al. 2008; Zhang et al. 2010). It has been shown that melt ponds contribute relatively more to the under-ice light field due to a higher pond transmittance of up to 0.12 (Nicolaus et al. 2010), whereas the present parameterization only comprises bare ice. However, bare ice dominates with a melt pond coverage of about 20% >88°N (Nicolaus et al. 2010), which leaves

Citation: *Polar Research* 2015, *34*, 23978, http://dx.doi.org/10.3402/polar.v34.23978

about 80% as bare ice. We observed further that melt ponds were nearly all refrozen and covered by a 1- to 2-cm-thick layer of ice at the time of our arrival at stations. For instance, melt pond transmittance was only 0.01 at station 248, with a 4-cm-thick cover of ice. We note that August–September is late regarding primary production so that differences in transmittance between bare ice and melt pond are insignificant, but earlier in the season the above relation can be applied for the 80% of the bare ice with no melt ponds.

Transmittance, attenuation and absorption

A photon budget for absorption of light in the water column below the ice was constructed based on the light spectrum leaving the bottom of the ice. The budget was constructed by calculating the total absorption coefficient at each wavelength ($a_{sum}(\lambda)$) by adding the measured absorption coefficients for phytoplankton (a_{phyto}), non-pigment particles (a_{det}), CDOM (a_{CDOM}) and the absorption coefficients for pure water from Pope & Fry (1997). The fraction of light absorption by each component at each wavelength was then calculated from Eqn. 1.

$$a_{sum}(\lambda) = a_w(\lambda) + a_{det}(\lambda) + a_{phyto}(\lambda) + a_{CDOM}(\lambda) \quad (1)$$

The fraction light over the PAR spectrum was then weighted by the irradiance at each wavelength according to Eqn. 2:

$$\text{Fraction absorbed by component } j = \sum_{\lambda=400}^{\lambda=700} fa_j(\lambda) * I_f(\lambda), \quad (2)$$

where fa_j is the fraction of the total absorption (a_{sum}) by component j and I_f is the fraction of I_{PAR} at the wavelength (sum of I_{PAR} from 400 to 700 nm = 1).

The photon budget showed that 4% of surface PAR was available at the bottom of the ice, and that only 3% of this light was absorbed by the phytoplankton in the water, with 30% for CDOM, 5% for non-pigmented material and 62% for water (Fig. 6). The calculations demonstrate that the low Arctic Ocean primary productivity is due to a high albedo, a low transmittance through the ice and only a small fraction (3%) of the light actually reaching the water column is absorbed by algae because of their low biomass. Instead, light is absorbed by water and CDOM. Thus, the system is light limited because the low light levels below the ice prevents the build-up of a significant algae biomass, which, in turn, indicates that there is less light for the phytoplankton compared to water and CDOM. As all light is eventually absorbed in a deep water column, except for the small fraction that is backscattered, there is a kind of "competition" between the

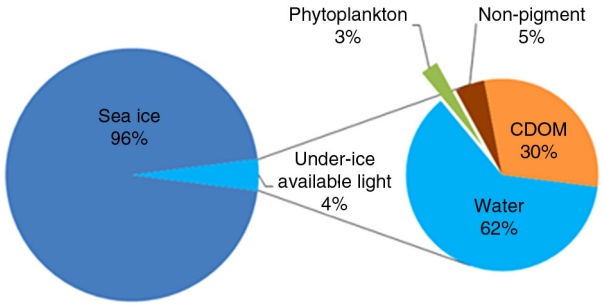

Fig. 6 Under-ice light partitioning for the central Arctic Ocean (>88°N). Coloured dissolved organic matter is abbreviated to CDOM.

light-absorbing agents for the light. The productivity of the system is determined by the ability of phytoplankton to build a biomass that can absorb the light before it is absorbed by other components (see Eqn. 1 and Markager & Vincent 2001). The effects of high absorption of light in the red part of the spectrum are present in all marine ecosystems, but the high concentrations of CDOM in combination with sea ice, and for part of the year, a low surface irradiance, indicate that the Arctic Ocean might be the most light limited of all the oceans. The spectral attenuation coefficient $K_d(\lambda)$ below the ice for stations 231 and 246 shows also the enhanced CDOM-related absorption in the blue part of the spectrum with absorption aw (m^{-1}) for pure water (Pope & Fry 1997) in comparison (Fig. 7). The terrestrial origin of the CDOM, shown above, identify the major Russian rivers as the sources of both freshwater and CDOM (Peterson et al. 2002). This implies that any changes in CDOM absorption in the Arctic Ocean will depend on river discharges and their catchment characteristics.

Chl-a absorption and absorbed light

Normalized spectral downwelling irradiance $E_d(\lambda)$ leaving from below the ice at the representative station 227 shows a clear maximum in the blue–green (480–510 nm

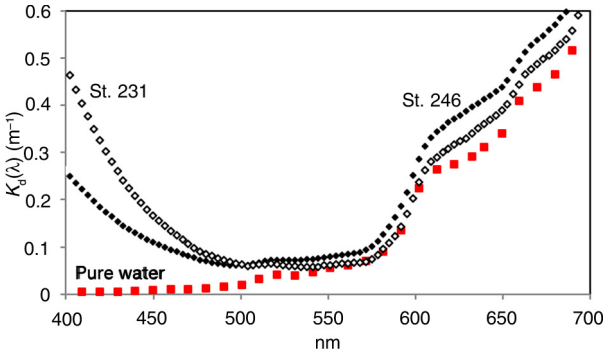

Fig. 7 Spectral attenuation coefficient $K_d(\lambda)$ (m^{-1}) at stations 231 and 246 and in pure water (Pope & Fry 1997).

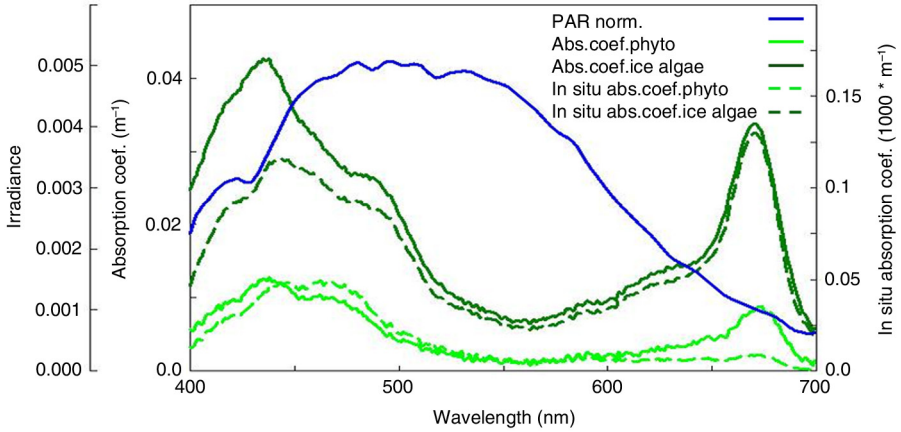

Fig. 8 Spectra of absorption coefficients (m^{-1}) for phytoplankton and ice algae. Spectral distribution of in situ absorption of light (m^{-1}) calculated as the absorption coefficient * fraction of PAR at the wavelength ($a(\lambda)$ * $I_f(\lambda)$). The blue line is the normalized (PAR = 1) spectrum below the ice.

and reduced values in the red and near-infra parts of the spectrum (Fig. 8). The average chl-a algae absorption $a_{ph}(\lambda)$ calculated for six stations for phytoplankton is typical for a diatom-dominated absorption spectra, with two clear absorption maxima around 435 and 670 nm, as well as the fucoxanthin or carotenoid "shoulder" around 470 nm (Falkowski & Raven 1997). For the ice algae the "shoulder" at 470 nm is less pronounced, indicating a lower content of accessory pigments. Spectral distribution of light absorbed by phytoplankton, expressed as the in situ absorption coefficient (Fig. 8), shows a high absorption in the blue region of the spectrum, and there is little light available for the phytoplankton above 600 nm due to the high absorption by water (Fig. 8). The absorption efficiency (A_e) was calculated for both phytoplankton and ice algae for both surface spectrum and the spectrum just below the ice, in order to evaluate and quantify acclimatization of the two populations (ice algae and phytoplankton) to the two light regimes. The A_e parameter is the ratio between the mean in situ absorption coefficient in a given spectrum (â) and the numerical mean of the absorption coefficient of phytoplankton (â)

$$A_e = a/(\hat{a}) \quad (3)$$

The A_e parameter expresses the matching of the absorption spectrum of a given phytoplankton population to the available light spectrum (Markager & Vincent 2001) and thereby a possible acclimatization to the prevailing light spectrum. The A_e value for ice algae decreases by 10% when they receive the under-ice spectrum compared to the surface spectrum (Table 2). The ice algae therefore do not seem to be spectrally acclimated to the light field under the ice. For phytoplankton, the difference is the other way. They increase the absorption efficiency by 8% in the under-ice spectrum compared to the surface spectrum. The difference is due to a more pronounced absorption around 470 nm compared to ice algae, so phytoplankton appear better acclimated to the bluish light spectrum below the ice than the ice algae (Fig. 8).

Conclusions

Average ice thickness in late summer 2012 in the central Arctic Ocean was lower by about 30 cm compared to a 2003–07 data set. Sea-ice transmittance was not correlated with sea-ice thickness but instead to a relatively higher backscattering in the air-filled channels as brine drainage was an important factor in the relatively warm ice. The PAR attenuation in the water under the ice was strongly governed by water and CDOM absorption as shown by both partitioning analyses. Only about 3% of the 4% transmitted light in the water column was utilized by the phytoplankton in the water. The CDOM showed a strong terrestrial origin indicating the Russian rivers as a main source. There were clear spatial differences in temperatures, salinity and CDOM absorption coefficients of the water just below the ice between stations of Pacific and Atlantic origin. This indicates a high degree of mixing between the Polar Mixed Layer and deeper lying water masses.

Table 2 The absorption efficiency—A_e—(dimensionless) for ice algae and phyto-plankton at surface and under-ice light spectrum, respectively.

	Surface spectrum	Under-ice spectrum
Ice algae	1.00	0.90
Phytoplankton	0.96	1.04

Citation: *Polar Research* 2015, *34*, 23978, http://dx.doi.org/10.3402/polar.v34.23978

Acknowledgements

Brødrene Hartmann's Foundation and the Carlsberg Foundation are thanked for their financial support. The helicopter team, captain and crew of icebreaker *Oden*, and not at least cruise leader Christian Marcussen, Geological Survey of Denmark, are all thanked for the successful LOMROG III cruise and very good cooperation.

References

Aagaard K., Weingartner T.J., Danielson S.L., Woodgate R.A., Johnson G.C. & Whitledge T.E. 2006. Some controls on flow and salinity in Bering Strait. *Geophysical Research Letters 33*, L19602, doi: 10.1029/2006GL026612.

Ardyna M., Babin M., Gosselin M., Devred E., Bélanger S., Matsuoka A. & Tremblay J.-É. 2013. Parameterization of vertical chlorophyll a in the Arctic Ocean: impact of the subsurface chlorophyll maximum on regional, seasonal, and annual primary production estimates. *Biogeosciences 10*, 4383–4404.

Arrigo K.R., Dijken V.G. & Sudeshna P. 2008. Impact of a shrinking Arctic ice cover on marine primary productivity. *Geophysical Research Letters 35*, L19603, doi: 10.1029/2008GL035028.

Arrigo K.R., Matria P.A. & Dijken G.L. 2011. Primary productivity in the Arctic Ocean: impacts of complex optical properties and subsurface chlorophyll maxima on large-scale estimates. *Journal of Geophysical Research—Oceans 116*, C11022, doi: 10.1029/2011JC007273.

Boetius A., Albrecht S., Bakker K., Beinhold C., Felden J., Fernandez-Méndez M., Hendricks S., Katlein C., Lalande C., Krumpen T., Nicolaus M., Peeken I., Rabe B., Rogacheva A., Rybakova E., Somavilla R. & Wenzhöfer F. 2013. Export of algal biomass from melting Arctic sea ice. *Science 339*, 1430–1432.

Bricaud A. & Stramski D. 1990. Spectral absorption coefficients of living phytoplankton and nonalgal biogenous matter: a comparison between the Peru upwelling area and the Sargasso Sea. *Limnology and Oceanography 35*, 562–582.

Cleveland L.S. & Weidemann A.D. 1993. Quantifying absorption by aquatic particles: a multiple scattering correction for glass-fiber filters. *Limnology and Oceanography 38*, 1321–1327.

Cox G.F.N. & Weeks W.F. 1983. Equations for determining the gas and brine volumes in sea-ice samples. *Journal of Glaciology 29*, 306–316.

Falkowski P.G. & Raven J.A. 1997. *Aquatic photosynthesis*. Oxford: Blackwell Science.

Fofonoff N.P. & Millard R.C. Jr. 1983. *Algorithms for computation of fundamental properties of seawater. UNESCO Technical Papers in Marine Science 44*. Paris: Division of Marine Sciences, United Nations Educational, Scientific and Cultural Organization.

Glud R.N., Rysgaard S., Kühl M. & Hansen J.W. 2007. The sea ice in young sound: implications for carbon cycling. In S. Rysgaard & R.N. Glud (eds.): *Carbon cycling in Arctic marine ecosystems: case study young sound. Meddelelser om Grønland, Bioscience 58*. Pp. 62–85. Copenhagen: Museum Tusculanum Press.

Gosselin M., Levasseur M., Wheeler P.A., Horner R.A. & Booth B.B. 1997. New measurements of phytoplankton and ice algal production in the Arctic Ocean. *Deep-Sea Research Part II 44*, 1623–1644.

Granskog M.A., Stedmon C., Dodd C.A., Amon R.M.W., Pavlov A.K., Steuer L. & Hansen E. 2012. Characteristics of colored dissolved organic matter (CDOM) in the Arctic outflow in the Fram Strait: assessing the changes and fate of terrigenous CDOM in the Arctic Ocean. *Journal of Geophysical Research—Oceans 117*, C12021, doi: 10.1029/2012JC008075.

Hamre B., Winther J.-G., Gerland S., Stamnes J. & Stamnes K. 2004. Modeled and measured optical transmittance of snow-covered first-year sea ice in Kongsfjorden, Svalbard. *Journal of Geophysical Research—Oceans 109*, C10006, doi: 10.1029/2003JC001926.

Hawes I., Lund-Hansen L.C., Sorrell B.K., Nielsen M.H., Borzák R. & Buss I. 2012. Photobiology of sea ice algae during initial spring growth in Kangerlussuaq, West Greenland: insights from imaging variable chlorophyll fluorescence of ice cores. *Photosynthesis Research 112*, 103–115.

Jones E.P., Anderson L.G., Jutterström S., Mintrop L. & Swift J.H. 2008. Pacific freshwater, river water and sea ice meltwater across Arctic Ocean basins: results from the 2005 Beringia Expedition. *Journal of Geophysical Research—Oceans 113*, C08012, doi: 10.1029/2007JC004124.

Kirk J.T.O. 1994. *Light and photosynthesis in aquatic ecosystems*. Cambridge: Cambridge University Press.

Kishino M., Takahashi M., Okami N. & Ichimura S. 1985. Estimation of the spectral absorption coefficients of phytoplankton in the sea. *Bulletin of Marine Sciences 37*, 634–642.

Kwok R. & Rothrock D.A. 2009. Decline in Arctic sea ice thickness from submarine and ICESat records: 1958–2008. *Geophysical Research Letters 36*, L15501, doi: 10.1029/2009GL039035.

Leppäranta M. & Manninen T. 1988. *The brine and gas content of sea ice with attention to low salinities and high temperatures. Finish Institute of Marine Research Internal Report 1988 (2)*. Helsinki: Finnish Institute of Marine Research.

Light B., Grenfell T.C. & Perovich D.K. 2008. Transmission and absorption of solar radiation by Arctic sea ice during the melt season. *Journal of Geophysical Research—Oceans 113*, C03023, doi: 10.1029/2006JC003977.

Lund-Hansen L.C. 2004. Diffuse attenuation coefficients Kd(PAR) at the estuarine North Sea–Baltic Sea transition: time-series, partitioning, absorption, and scattering. *Estuarine, Coastal, and Shelf Science 61*, 251–259.

Lund-Hansen L.C., Nielsen J.M., Blüthgen J., Hai D.N., Nielsen M.H. & Lam N.N. 2013. Estuarine morphometry governs optically active substances, Kd(PAR) and beam

attenuation: assessments from a tropical ria and a temperate coastal plain estuary. *Hydrobiologia 156*, 234–244.

Markager S. & Vincent W. 2001. Light absorption by phytoplankton: development of a matching parameter for algal photosynthesis under different spectral regimes. *Journal of Plankton Research 23*, 1373–1384.

Maslanik J.A., Fowler C., Stroeve J., Drobot S., Zwally J. & Emery W. 2007. A younger, thinner Arctic ice cover: increase potential for rapid extensive sea-ice loss. *Geophysical Research Letters 34*, L24501, doi: 10.1029/2007GL032043.

Nicolaus M., Gerland S., Hudson S.R., Hanson S., Haapala J. & Perovich D. 2010. Seasonality of spectral albedo and transmittance as observed in the Arctic Transpolar Drift in 2007. *Journal of Geophysical Research—Oceans 115*, C11011, doi: 10.1029/2009JCO006074.

Nicolaus M., Katlein C., Maslanik J. & Hendricks S. 2012. Changes in Arctic sea ice result in increasing light transmittance and absorption. *Geophysical Research Letters 39*, L24501, doi: 10.129/2012GL053738.

Ogi M. & Rigor I.G. 2013. Trends in Arctic sea ice and the role of atmospheric circulation. *Atmospheric Science Letters 14*, 97–101.

Parkinson C.L., Cavalieri D.J., Gloersen P., Zwally J.H. & Comiso J.C. 1999. Arctic sea ice extents, areas, and trends, 1978–1996. *Journal of Geophysical Research—Oceans 104*, 20837–20856.

Parkinson C.L. & Comiso J.C. 2013. On the 2012 record low Arctic sea ice cover: combined impact of preconditioning and an August storm. *Geophysical Research Letters 40*, 1356–1361.

Perovich D.K. 1996. *The optical properties of sea ice*. CRREL *Monograph 96-1*. Hanover, NH: US Army Corps of Engineers.

Perovich D.K., Cota G.F., Maykut G.A. & Grenfell T.C. 1993. Bio-optical observations of first-year Arctic sea ice. *Geophysical Research Letters 20*, 1059–1062.

Peterson B.J., Holmes R.M., McClelland J.W., Vörösmarty C.J., Lammers R.B., Shiklomanov A.I., Shiklomanov I.A. & Rahmstorf S. 2002. Increasing river discharge to the Arctic Ocean. *Science 298*, 2171–2173.

Pope R.M. & Fry E.S. 1997. Absorption spectrum (380–700 nm) of pure water. II. Integrating cavity measurements. *Applied Optics 36*, 8710–8723.

Popova E.E., Yool A., Coward A.C., Dupont F., Deal C., Elliott S., Hunke E., Jin M., Steele M. & Zhang J. 2012. What controls primary production in the Arctic Ocean? Results from an intercomparison of five general circulation models with biogeochemistry. *Journal of Geophysical Research—Oceans 117*, C00D12, doi: 10.1029/2011JC007112.

Rigor I.G. & Wallace J.M. 2004. Variation in the age of Arctic sea-ice and summer sea-ice extent. *Geophysical Research Letters 31*, L09401, doi: 10.1029/2004GL019492.

Riihelä A., Laine V., Manninen T., Palo T. & Vihma T. 2010. Validation of the Climate–SAF surface broadband albedo product: comparisons with in situ observations over Greenland and the ice-covered Arctic Ocean. *Remote Sensing of the Environment 114*, 2779–2790.

Rothrock D.D., Yu Y. & Maykut G.A. 1999. Thinning of the Arctic sea-ice cover. *Geophysical Research Letters 26*, 3469–3472.

Rudels B., Jones E.P., Shauer U. & Erikson P. 2004. Atlantic sources of the Arctic Ocean surface and halocline waters. *Polar Research 23*, 181–208.

Sakshaug E. 2004. Primary and secondary production in the Arctic Seas. In R. Stein & R.W. Macdonald (eds.): *The organic carbon cycle in the Arctic Ocean*. Pp. 57–81. Berlin: Springer.

Schauer U., Rudels B., Jones E.P., Anderson L.G., Muench R.D., Björk G., Swift J.H., Ivanov V. & Larsson A.-M. 2002. Confluence and redistribution of Atlantic water in the Nansen, Amundsen and Makarov basins. *Annals of Geophysics 20*, 257–273.

Stæhr P.A. & Markager S. 2004. Parameterization of the chlorophyll a specific in vivo light absorption coefficient covering estuarine, coastal and oceanic waters. *Journal of Remote Sensing 25*, 5117–5130.

Stedmon C. & Markager S. 2001. The optics of chromophoric dissolved organic matter (CDOM) in the Greenland Sea: an algorithm for differentiation between marine and terrestrial derived organic matter. *Limnology and Oceanography 46*, 2087–2093.

Stroeve J.C., Serreze M.C., Fetterer F., Arbetter T., Meier W. & Maslanik J. 2005. Tracking the Arctic's shrinking ice cover: another extreme September minimum in 2004. *Geophysical Research Letters 32*, L04501, doi: 10.1029/2004GL021810.

Thomas D.N. & Dieckmann G.S. 2002. Antarctic sea ice—a habitat for extremophiles. *Science 295*, 641–644.

Tucker W.B., Gow A.J., Meese D.A. & Bosworth H.W. 1999. Physical characteristics of summer sea ice across the Arctic Ocean. *Journal of Geophysical Research—Oceans 104*, 1489–1504.

Vihma T., Jaagus J., Jakobson E. & Palo T. 2008. Meteorological conditions in the Arctic Ocean in spring and summer 2007 as recorded on the drifting ice station TARA. *Geophysical Research Letters 35*, L18706, doi: 10.1029/2008GL034681.

Warner K., Iacozza J., Scharien R. & Barber D. 2013. On the classification of melt season first-year and multi-year sea ice in the Beaufort Sea using Radarsat-2 data. *International Journal of Remote Sensing 34*, 3760–3774.

Zhang J., Spitz Y.H., Steele M., Ashjian C., Campbell R., Berline L. & Matria P. 2010. Modeling the impact of declining sea ice on the Arctic marine planktonic ecosystem. *Journal of Geophysical Research 115*, C10015, doi: 10.1029/2009JC005387.